Helically Wrapped Supercoiled Polymer (HW-SCP) Artificial Muscles: Design, Characterization, and Modeling

Thulani Tsabedze, Christopher Mullen, Ryan Coulter, Scott Wade and Jun Zhang

Abstract-Supercoiled polymer (SCP) artificial muscles exhibit many desirable properties such as large contractions and high power density. However, their full potential as robotic muscles is challenged by insufficient strain or force generation - non-mandrel-coiled SCP actuators produce up to 10-20% strain; mandrel-coiled SCP actuators often lift up to 10-30g of weight. It is strongly desired but difficult to obtain SCP actuators that produce large strain and large force. In this paper, the design, characterization, and modeling of helically wrapped SCP (HW-SCP) actuators are presented, which can produce up to 40-60% strain and lift more than 90g of weight. By adjusting their configuration parameters, their strain and force performance can be changed. Experiments are conducted to characterize the force production, strain, and speed of HW-SCP actuators. A Preisach hysteresis model and a polynomial model are adopted to accurately capture the actuator behaviors. This work contributes to high-performance artificial muscles.

I. INTRODUCTION

With robots growing more ubiquitous, increasing demands exist for new lightweight materials and actuators that are safer and less costly than conventional motor systems [1]. Artificial muscles, which will power robots of the future, are broadly defined as materials and devices that can change their shapes under external stimuli [2]–[4].

As an emerging artificial muscle technology, supercoiled polymers (SCP) actuators has attracted a tremendous amount of interest among the robotics community. SCP actuators exhibit high energy-density to weight ratio, inherent compliance, large strain, and are lightweight and low-cost [3], [5]. Since first created [5], SCP actuators have been explored in many robotic applications, such as robotic fingers, hands, and arms [6]–[8], soft robots [9], assistive robots [10], and wearable devices [11]. SCP actuators are fabricated by twisting and coiling polymer threads or filaments, such as nylon sewing threads. Two fabrication approaches have been widely adopted: non-mandrel-coiling and mandrel-coiling.

Non-mandrel-coiled SCP actuators, as shown in Fig. 1(a), can be efficiently manufactured with coiling and heat treatment [5], [8]. Unfortunately, they do not perform well at low tension conditions [5], [12]. The pretension requirement of non-mandrel-coiled SCP actuators limits the adaptability and creates difficulty in obtaining movement in robotic systems. For example, the tension from the muscles is often

This work is supported in part by the National Science Foundation under Grant Number 1852578

Thulani Tsabedze, Christopher Mullen, Ryan Coulter and Jun Zhang are with the Department of Mechanical Engineering, University of Nevada, Reno, NV 89557, USA (email: thulanit@nevada.unr.edu; volkcm@nevada.unr.edu; rcoulter@nevada.unr.edu; jun@unr.edu.)

Scott Wade is with the Department of Mechanical Engineering, Boston University, Boston, MA 02215, USA (email: stwade@bu.edu.)

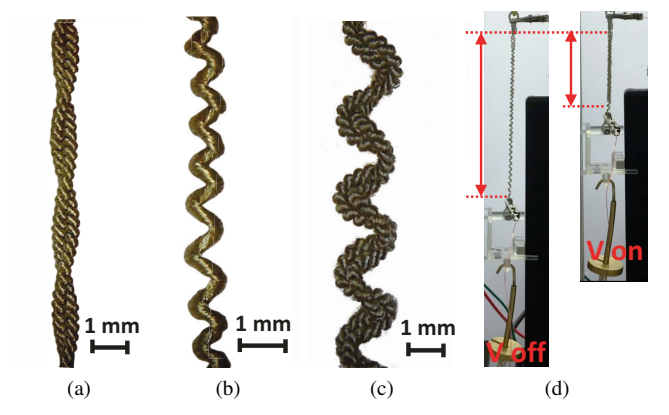


Fig. 1. The coiled structure of (a) a non-mandrel-coiled and (b) a mandrel-coiled supercoiled polymer (SCP) actuator. (c). A helically-wrapped (HW)-SCP actuator. (d). Live actuation of an HW-SCP actuator. Over 50% strain was generated.

transferred into the system [12]. For applications in assistive robots, the pretension requirements lower the comfort level of the wearer. Furthermore, non-mandrel-coiled SCP actuators often can only generate strains up to 10-20% [8], [13], limiting the possible range of robot motion. It is believed that the reason of small strain of non-mandrel-coiled SCP actuator is due to the close distance among adjacent coils [8]. Nonetheless, non-mandrel-coiled SCP actuators have good force output. A regular actuator with around 1 mm diameter could generate over 1 N of force [14], [15].

Mandrel-coiled SCP actuators, as shown in Fig. 1(b), are fabricated by wrapping twisted polymer threads around a mandrel to create coils [5], [9]. These actuators can generate strain up to 49% or larger, do not require pretension [5], [16], [17]. However, a major drawback is their low stiffness – they often generate a small force, cannot support substantial load, and the coil structures are fragile, limiting their practical application potential. A reason of weakness of mandrel-coiled SCP actuator is likely due to the low-stiffness of polymer threads [5]. A regular mandrel-coiled SCP actuator often only generate around or less than 0.1-0.3 Newton of force [5], [17], [18]. While large strain is appealing, the small stiffness of mandrel-coiled SCP actuators may significantly challenge its use in real-world scenarios.

The motivation of this study is to create a new type of SCP actuators that can exert large forces and large range of motion. In this study, we propose a helically wrapped (HW)-SCP actuator, as shown in Fig. 1(c). The main idea is to modify the manufacturing process so that HW-SCP

actuators exhibit the advantages of both non-mandrel-coiled and mandrel-coiled SCP actuators. The HW-SCP actuator is created by wrapping a regular non-mandrel-coiled SCP actuator around a mandrel to form a helically coiled structure. Thus the HW-SCP actuator has a controllable distance among adjacent coils and has a large stiffness. The effects of actuator parameters (inner diameter, pitch, diameter of the non-mandrel-coiled SCP diameter) on the strain and force performance of the HW-SCP actuators are studied. Our preliminary tests show that HW-SCP actuators generate superior performance over existing ones - they retain the impressive strains of mandrel-coiled SCP actuator, and overcome the low strength and inherent fragility. These new actuators can achieve strain up to 40-60% with respect to the initial loaded length, as shown in Fig. 1(d). Meanwhile, they can actuate whilst bearing large loads comparable to that of non-mandrel-coiled SCP actuators.

II. DESIGN AND FABRICATION

A. Proposed Design

In this study, the design space of HW-SCP actuators consists of three parameters, namely the inner diameter, s, the pitch p, and the diameter of the initial SCP actuator before wrapping, d, as shown in Fig. 2(a). A few fabricated sample HW-SCP actuators with different configuration parameters are shown in Fig. 2(b).

The inner diameter, *s*, equals the diameter of the mandrel used during actuator fabrication. By modifying the mandrel sizes (Section II.B and Section IV.A), the inner diameter of HW-SCP actuators can be changed. It is expected that smaller mandrel sizes increase the stiffness of the actuator.

The pitch, p, is the distance between two successive coils. The pitch can either be designed in the actuator fabrication process (details in Section II.B) or modified under different loading conditions. It is expected that changing the pitch will influence the force and strains performance of the HW-SCP actuators. For example, if the pitch is very large, then the actuator resembles a non-mandrel-coiled SCP actuator, and will have a small amount of contraction.

The diameter of the initial SCP actuator before wrapping, d, can be modified by changing the ply number, which is the number of thin polymer threads used for SCP actuator fabrication. In this study, silver plated nylon 66 threads (110/34 dtex Z turns High Conductive Yarn, V Technical Textiles) were employed. Increasing the ply number increases the diameter of the SCP actuator.

B. Fabrication Procedure

The fabrication process consists of 4 steps, and a schematic of the process is shown in Fig. 2(c).

1) Step 1: Coiling (Non-mandrel): To start off, regular non-mandrel coiled SCP structure is manufactured. Following our previous approaches [14], [19], a nylon thread is attached to a motor and a suspended weight for twist insertion. The load is picked to be large enough that the thread remains taut but small enough not to lead to rupture. The motor is spun until the thread is fully coiled. This coiled

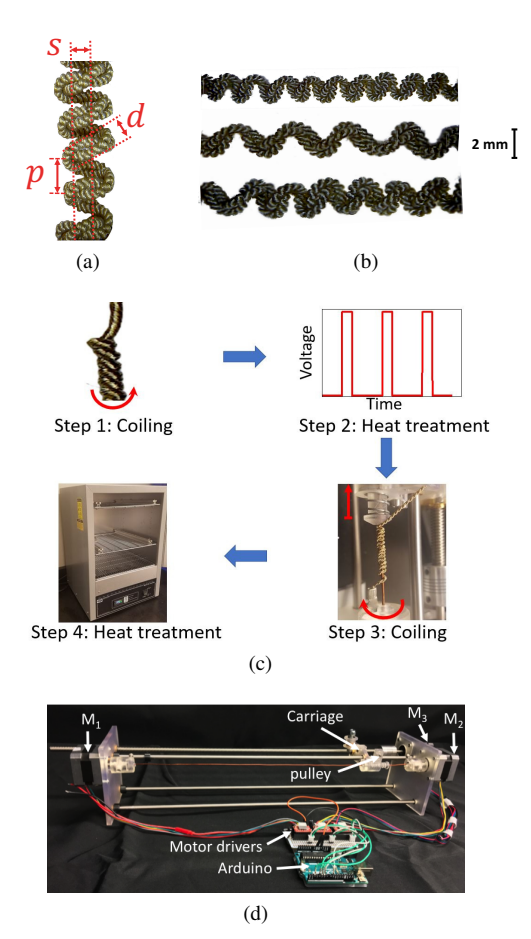


Fig. 2. (a) The design parameters of the HW-SCP actuator. (b) Samples of fabricated HW-SCP actuators with different parameters. (c) The manufacturing process of HW-SCP actuators. (d) A custom-made mandrel fabricator.

thread is double-backed to balance the torque from twist insertion, stabilizing the coiled structure.

- 2) Step 2: Heat Treatment (Joule Heating): The coiled structure formed by twist insertion is heat treated by the process of Joule heating, wherein a voltage is applied across the coiled thread while a load is suspended [5], [8]. During this process the coiled thread elongates plastically. Once it no longer elongates, around 10% strain can be achieved, and a non-mandrel-coiled SCP actuator is created. During our preliminary testing, it was found that HW-SCP actuators manufactured without this step exhibited poor performance.
- 3) Step 3: Coiling (Mandrel): To manufacture HW-SCP actuators, the non-mandrel-coiled SCP actuator is further helically wrapped around a mandrel using a custom-made fabricator shown in Fig. 2(d). In this step, the pitch and inner diameter of the manufactured HW-SCP actuator can be modified. For example, if the smallest possible pitch is desired, the specified pitch on the mandrel fabricator will be set equal to the diameter of the initial SCP actuator.
- 4) Step 4: Heat Treatment (Oven): Finally, the mandrel-wrapped SCP actuator is placed in an oven to stabilize the coil structure. The time and temperature for heat treating are determined empirically. The ideal annealing temperature is above the operating temperature of the actuator, but below

the melting temperature. Same as [5], both contraction and elongation motions can be obtained by changing the coils chirality. In this study, we mainly study the contraction performance of HW-SCP actuators.

C. Fabrication Results

In this study, HW-SCP actuators with different inner diameters (s), pitches (p), and diameter of initial SCP actuators before wrapping (d) were fabricated.

Three different inner diameters of HW-SCP actuators, 0.13 mm, 0.25 mm, and 0.51 mm were manufactured. Furthermore, initial SCP actuators with different ply numbers (4, 6, and 8) before wrapping were adopted. The diameters of 4, 6 and 8-ply non-mandrel-coiled SCP actuators were 0.90 mm, 1.11 mm, and 1.34 mm, respectively. By employing these SCP actuators, the diameters of the corresponding HW-SCP actuators (inner diameter: 0.51 mm) were approximately 2.57 mm, 2.70 mm, and 2.95 mm.

III. MODELING

In this section, three modeling approaches, namely, linear dynamical model, polynomial model, and Preisach hysteresis model, are briefly reviewed. More details of these approaches can be found in [8], [14], [19]–[24].

A. Linear Dynamical Model

The thermo-mechanical properties of SCP actuators can be approximately described as [8]

$$F = k_1(x - x_1) + k_2 \dot{x} + k_3(T - T_0), \tag{1}$$

where F is the force output, x and x_I are the current and resting length of the actuator, respectively, k_1 denotes the stiffness, k_2 is a damping term, T is the actual temperature of the actuator, T_0 is the ambient temperature, and k_3 represents the force change per unit temperature.

The thermal dynamics behave roughly as a first-order linear system [8], [14]:

$$C\frac{dT}{dt} = P(t) - \lambda(T - T_0), \tag{2}$$

where C is thermal mass, λ is the absolute thermal conductivity, and P is the input electrical power. The time constant of the system is $\tau = \frac{C_{\text{th}}}{\lambda}$.

B. Polynomial Model

A polynomial model can be employed:

$$O_{\text{linear}}(I) = p_n I^n + \dots + p_2 I^2 + p_1 I + p_0,$$
 (3)

where O_{linear} denotes the actuator output, p_k, \dots, p_1, p_0 are constants, I is the input to the actuator, and n is the order of the polynomial. It has been shown that the force-power input correlation of SCP actuators is approximately linear [14], [25]. Furthermore, this model can be identified using MATLAB command *polyfit* with a small computational cost.

C. Preisach Hysteresis Model

Hysteresis, as a common type of nonlinearity, appears in most artificial muscles [3], [26]. A number of recent studies confirmed and analyzed the hysteresis in SCP actuators [19], [27]–[29]. It is thus expected that hysteresis also appears in HW-SCP actuators in this study.

The Preisach model is one of the most widely adopted approaches to capture hysteresis behaviors. The output of the model, O_{Preisach} , can be written as follows:

$$O_{\text{Preisach}}(I) = \sum_{i=1}^{L} \sum_{j=1}^{L+1-i} \mu_{ij} s_{ij}(I) + b_0,$$
 (4)

where μ_{ij} is the model parameter called the Preisach weight, $s_{ij}(I)$ is determined by the input history, L is the level of discretization, b_0 is a constant bias. The model can be efficiently identified using MATLAB command *lsqnonneg* as linear least-squares approach can be used [19].

IV. EXPERIMENTAL SETUP

A. Fabrication of Individual SCP Actuator

- 1) Non-mandrel-coiled SCP actuator: Following our previous study [14], nylon threads were twisted until fully coiled using a motor. For an 8-ply actuator, a load of 150 g was utilized during twist insertion. The heat treating was done in approximately 10 cycles of voltage pulses (3s on, 50s off). In the end, 10-15% repeatable strain was obtained.
- 2) Mandrel-coiled SCP actuator: By wrapping threads to a mandrel fabricator, such as the one shown in Fig.2(d), a mandrel-coiled SCP actuator can be created [5], [9]. In this study, we wrapped the non-mandrel-coiled SCP actuators to mandrels. The wrapped non-mandrel SCP actuator was placed in an oven for 1 hour at 180°C.

The working mechanism of the mandrel fabricator can be described as follows: It consists of three stepper motors, with M_1 and M_2 spinning in opposite directions. These motors spin the mandrel at a constant speed. M_3 is attached to a lead screw that drives the carriage left or right. The carriage consists of a spring-loaded pusher and a pulley for feeding SCP actuators into the mandrel. The pulley ensures there is minimal friction on the SCP actuator as it is being wound. To control the pitch, the speed of M_3 is adjusted accordingly.

B. Experimental Apparatus

Two experimental setups were used to conduct characterization of HW-SCP actuators for strain and force outputs.

1) Strain versus Voltage: As Fig. 3(a) shows, the strain of the HW-SCP actuators was measured using a position sensor (SPS-L225-HALS, Honeywell), which has a sensing range of 225 mm and resolution of 0.14 mm. A magnet was attached to the end of the actuator. A magnet holder was designed to allow the ease of changing the loads applied to the muscles with negligible induced friction. When the actuator was contracted, the sensor measured the position of the magnet. Similar to our previous study [19], a blower fan (Mechatronics MD4028V12B-RSR) was installed and applied at 3.20 V to provide even airflow, since pockets of hot air were otherwise spotted.

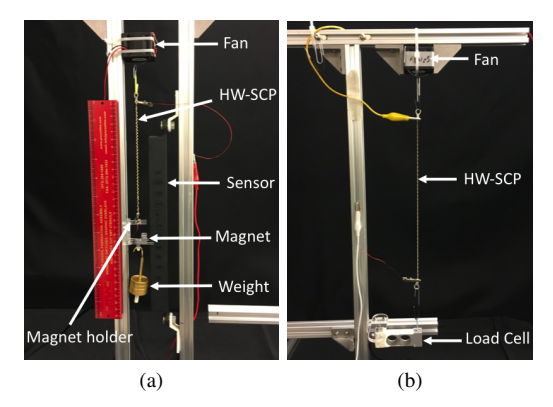


Fig. 3. The experimental setups for measuring (a) strain and (b) force of HW-SCP actuators.

2) Force versus Voltage: Fig. 3(b) shows the setup for force-voltage measurements. Similar to the case for strain measurement, one end of the HW-SCP actuator was attached below the fan with the same model and operating condition. The distal end was attached to a load cell (LSP-2, Transducer Techniques). The force signal was sent to LabVIEW USB-6001 data acquisition device. The position of the load cell can be adjusted in the beginning of each run, giving the flexibility to change the pretension. The input voltage was generated with an Arduino circuit.

V. EXPERIMENTAL RESULTS

A. Metric

The strain is used for comparing contractions of HW-SCP actuators with different configurations. In this study, the strain, Δx_u , is defined as

$$\Delta x_u = \frac{x - x_l}{x_l} \times 100\%,\tag{5}$$

where x is the actual length of the actuator, and x_l is the length of the actuator under a constant loading with no applied electric power. According to this definition, the strain will always be smaller than 100% when the actuator is contracted. It is noted that several existing studies adopted the resting length of actuators in strain calculation [5], [14], [30]. In our study, it was found that the resting length of HW-SCP actuator showed dependence on the previously applied electric power history, thus an exact resting length was difficult to obtain. The modeling accuracy was quantified by the average absolute error and the standard deviation error.

B. General Procedure

Each Strain-Voltage and Force-Voltage experiment was performed by applying a series of input voltage steps. The step sequence first monotonically increased from zero to maximum, and then decreased to zero, as shown in Fig. 4 (top). Similar input sequences have been chosen to measure the behaviors of SCP actuators [14], [19]. The maximum input was chosen based on a number of extreme tests, where the maximum voltages were attempted to be applied until the muscle burnt out. The maximum voltage chosen

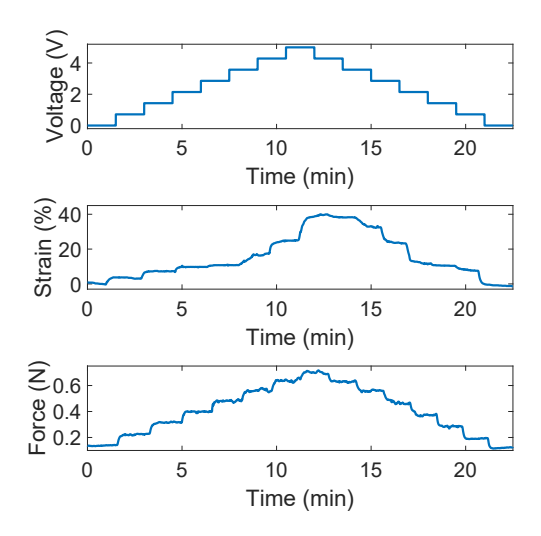


Fig. 4. Experimental measurements of HW-SCP actuators. Voltage input (top), strain (middle), and force transient responses (bottom).

for experiment operation was then placed at around 0.2 V less than the determined burnout voltage. This procedure was repeated for each loading condition to ensure that the maximum actuation range was obtained.

Both the transient and steady-state performances of HW-SCP actuators were studied. To measure the output response, each step was held for 90 seconds. Similar procedures were successfully employed to study the performance of SCP actuators [12], [19]. To obtain the steady-state strain and force values, the last 10-15 seconds of the output responses under each step were averaged. An example of the procedure is shown in Fig. 4, where samples of voltage input sequence, transient strain and force outputs are provided. It was noted that the data showed mild fluctuations, which might be caused by the ambient noisy environment, or the non-uniform conductive coating of the nylon threads. Accounting for noise and disturbances were beyond the scope of this work.

C. Strain Versus Voltage

The strains of HW-SCP actuators with different inner diameters (s = 0.13 mm, 0.25 mm, and 0.51 mm) were tested under three loading conditions, namely, 0.343 N, 0.637 N, and 0.931 N. These loading conditions were realized by hanging 35g, 65g, and 95g of weights to the actuator. It is noted that under a higher loading, the maximum applied voltage was larger. This is due to the fact that the HW-SCP actuator has a higher resistance when it is elongated.

Fig. 5(a)-(c) shows the steady-state lengths for the tested HW-SCP actuators under different voltage inputs. Large contraction was observed. For example, for the HW-SCP actuator with an inner diameter of 0.13 mm and under 0.343 N loading force, the length of the initial loaded actuator was 10.5 cm. The actuator contracted to 5.6 cm under 5 Volts voltage input. The strain-voltage measurements showed evident hysteresis, especially under low loads. This is consistent with existing studies [19], [27].

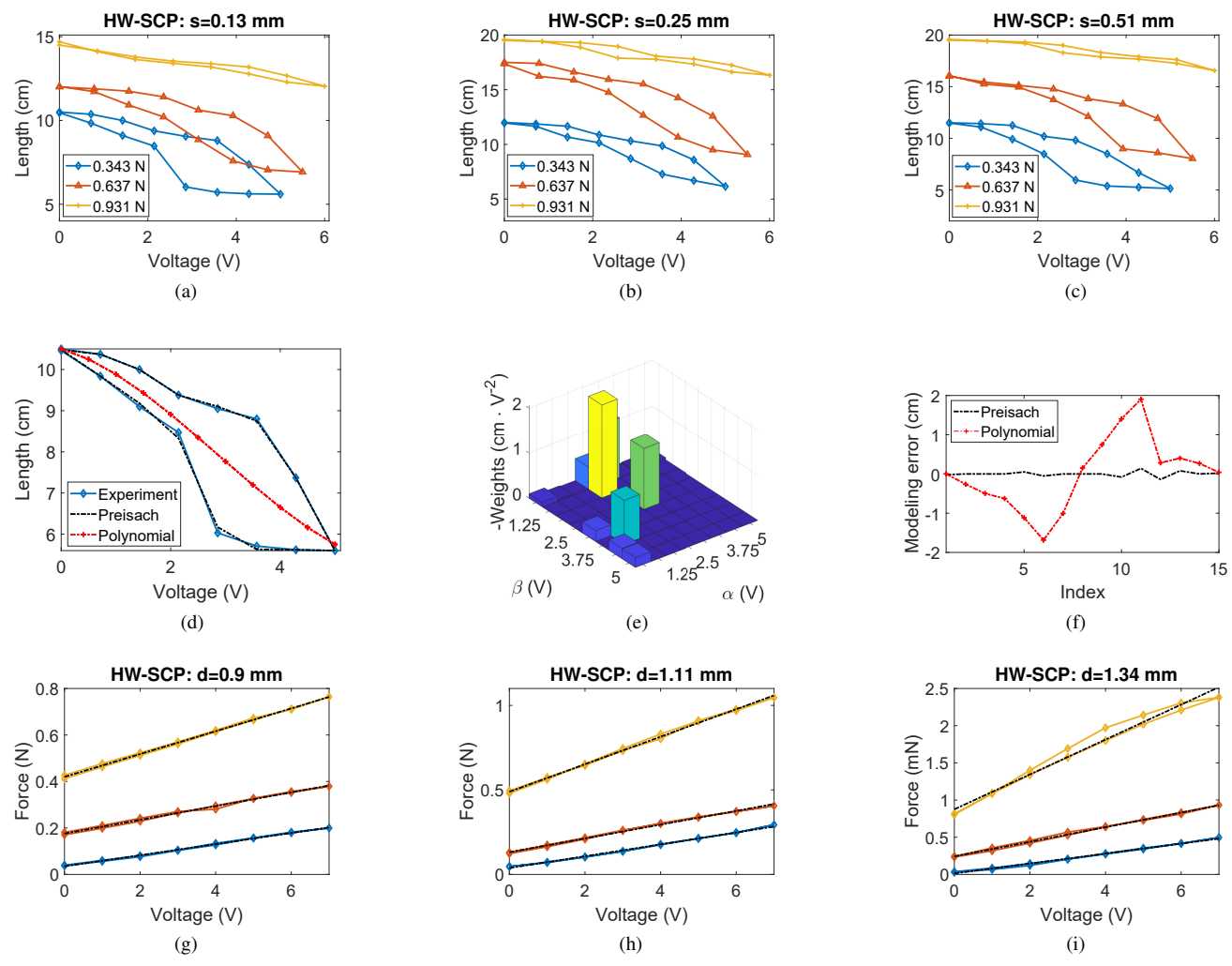


Fig. 5. Steady-state strain versus voltage for each HW-SCP actuator: (a) s = 0.13 mm, (b) s = 0.25 mm, and (c) s = 0.51 mm under three constant loading conditions. (d). The performance of a polynomial model and a Preisach model for strain-voltage of HW-SCP actuator (s = 0.13 mm). (e). The identified Preisach weights. (f). The modeling error comparison of the polynomial model and Preisach model. Steady-state force versus voltage for each HW-SCP actuator: (g) d = 0.9 mm, (h) d = 1.11 mm, and (i) d = 1.34 mm under three pretensions. The dashed lines denote the 1st-order polynomial model.

A third-order polynomial model and a Preisach model were employed to capture the strain-voltage measurements. Fig. 5(d)-(f) shows the modeling performances for the HW-SCP actuator (s = 0.13 mm, loading = 0.343 N). As shown, the Preisach model could accurately capture the pronounced hysteresis behavior of the HW-SCP actuator. The modeling errors of the polynomial model and Preisach model were 0.6929 ± 0.6034 cm and 0.0391 ± 0.0765 cm, respectively. The discretization level, L, of the Preisach model was chosen to be 8, $b_0 = 8.04$ cm, and the Preisach model weight is shown in Fig. 5(e).

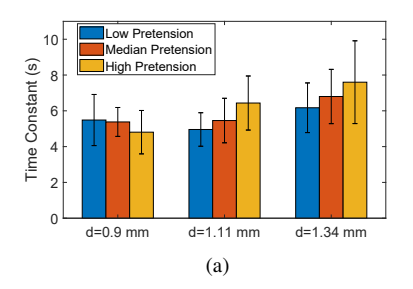
Due to the evident advantage of the Presiach model, it was further adopted to capture the length-voltage measurements of HW-SCP actuators with different configurations and under different loading conditions. For example, the modeling errors for the HW-SCP actuators (s=0.25 mm) were 0.0027 \pm 0.008 cm, 0.0088 \pm 0.0266 cm, and 0.0089 \pm 0.0210 cm for loading conditions of 0.343 N, 0.637 N, and 0.931 N, respectively.

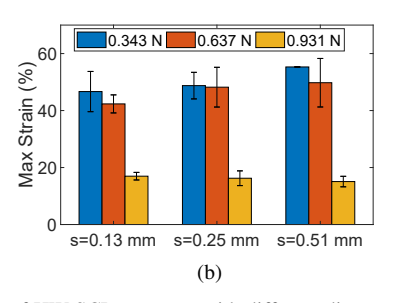
D. Force Versus Voltage

The forces of HW-SCP actuators with different initial SCP actuator diameters before wrapping (d=0.9 mm, 1.11 mm, and 1.34 mm) were tested under three pretensions. Pretension was generated by fixing the actuator's length longer than its resting length. Note HW-SCP actuator's pitch becomes larger under a higher pretension. Fig. 5(g)-(i) shows the steady-state forces under different voltage inputs. Unlike the strain measurements, the force-voltage measurements showed good linearity, consistent with existing studies [25]. First-order polynomials were employed to accurately capture the correlations, and the corresponding modeling performance and identified model parameters were summarized in Table I.

E. Dynamics

The heating and cooling time constants were measured based on the force versus voltage experimental data as a metric to quantify actuation speed, as shown in Fig. 6(a). It shows that the time constants were around 5s, relatively fast





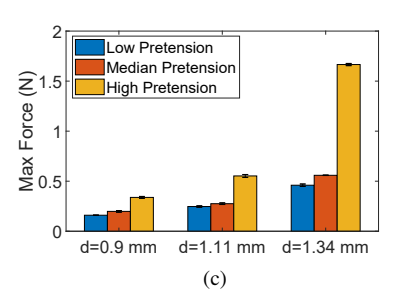


Fig. 6. (a) Time constants during heating and cooling of HW-SCP actuators with different diameters and under different pretensions. (b) Maximum strains of HW-SCP actuators of different inner diameters and under different loading conditions. (c) Maximum force output of HW-SCP actuators of different SCP diameters and under different pretensions.

considering that the diameters were around 2-3 mm. There were slight increases in the time constants as pretension and SCP diameter increase. Intuitively, this makes sense since increasing the diameter of the SCP actuators will increase the time needed for the actuator to cool down. The effects of the pretension to the time constants were not clear.

F. Effects of Actuator Configuration

As Fig. 6(b) shows, when the inner diameter of the HW-SCP actuator was fixed, the actuator generated larger strain under a smaller loading. This is likely because HW-SCP actuators under small loading resemble mandrel-coiled SCP actuators that can generate large contractions. Under large loading, the coils generated by the mandrel would become apart, thus making them resemble non-mandrelcoiled SCP actuators that can generate 10-15% strain. It also shows that by increasing the inner diameter, the HW-SCP actuator generated more strain under low loads and less strain under high loads, compared to the one with a smaller inner diameter. This is likely due to the stiffness change with inner diameters. With a larger inner diameter, the stiffness of the actuator decreases. Thus HW-SCP actuators with a larger inner diameter behaves more similar to non-mandrel-coiled SCP actuators under high loads.

Fig. 6(c) shows that HW-SCP actuators with larger diameters of initial SCP actuators without wrapping generated larger force outputs. This is due to the fact that the overall diameter and force generation of the HW-SCP actuator are

TABLE I

IDENTIFIED PARAMETERS OF THE FIRST-ORDER POLYNOMIALS.

	p_1	p_0	error
HW-SCP ($d = 0.9 \text{ mm}$):			
Low pretension	0.0239	0.0348	0.0029 ± 0.0014
Median pretension	0.0295	0.1758	0.0047 ± 0.0032
High pretension	0.0491	0.4197	0.0048 ± 0.0025
HW-SCP ($d = 1.11 \text{ mm}$):			
Low pretension	0.0350	0.0378	0.0041 ± 0.0035
Median pretension	0.0408	0.1313	0.0052 ± 0.0029
High pretension	0.0814	0.4891	0.0081 ± 0.0048
HW-SCP ($d = 1.34 \text{ mm}$):			
Low pretension	0.0668	0.0133	0.0094 ± 0.0008
Median pretension	0.0983	0.2421	0.0114 ± 0.0089
High pretension	0.2346	0.8753	0.0587 ± 0.0485

positively correlated to that of the initial SCP actuators. It was also observed that under a higher pretension, the actuator could generate a larger range of force outputs.

Fig. 6 shows the reproduceability of actuator performance based on three repeating experiments, where the force performance presents superior repeatability, and the dynamics and strain show noticeable variations.

VI. DISCUSSION AND CONCLUSION

In this study, a new HW-SCP actuator was proposed that can generate large strain and large force outputs. Multiple configurations (inner diameter, pitch, and the diameter of the initial SCP actuator before wrapping) of HW-SCP actuators have been designed and manufactured. The strain and force outputs under varying voltage steps of varying magnitudes were obtained. The time constants of the HW-SCP actuators were experimentally measured. A polynomial model and a Preisach hysteresis model were successfully employed to accurately capture the actuator behaviors.

As acknowledged in [3], while SCP actuators have attracted a lot of attention, more design studies are needed to improve their actuation capabilities. For instance, a widely-acknowledged challenge in soft robotics is to obtain large compliant deformations with small pretension. HW-SCP actuators exhibit key advantages in both strain and force, thus showing strong promise as an enabling compliant actuation technology. Furthermore, like mandrel-coiled SCP actuators, HW-SCP actuators do not require pretension and can cool quickly. This makes them well suited for applications where high-frequency actuation and compliance are desirable, such as assistive and rehabilitative devices.

The findings of this work serve as the first step of obtaining high-performance SCP actuators with fully controllable design spaces by striking a balance of the advantages of non-mandrel-coiled SCP actuator's high-force output and mandrel-coiled SCP actuator's appreciably large strain output. More in-depth numerical and physical studies can be conducted to understand how to design HW-SCP actuators and how the design parameters influence the overall actuator performers. With future studies, HW-SCP actuators can be designed for various applications and scenarios, making them truly versatile and attractive.

REFERENCES

- [1] H. Christensen and et. al., A Roadmap for US Robotics: From Internet to Robotics. 2016 Edition, 2016.
- [2] B. Tondu, "What is an artificial muscle? A systemic approach." Actuators, vol. 4, no. 4, p. 336, 2015.
- [3] J. Zhang, J. Sheng, C. O'Neill, C. J. Walsh, R. J. Wood, J. H. Ryu, J. P. Desai, and M. C. Yip, "Robotic artificial muscles: Current progress and future perspectives for biomimetic actuators," *IEEE Transactions on Robotics*, vol. 35, no. 3, pp. 761–781, 2019.
- [4] S. M. Mirvakili and I. W. Hunter, "Artificial muscles: Mechanisms, applications, and challenges," *Advanced Materials*, vol. 30, no. 6, p. 1704407, 2017.
- [5] C. S. Haines, M. D. Lima, N. Li, G. M. Spinks, J. Foroughi, J. D. W. Madden, S. H. Kim, S. Fang, M. Jung de Andrade, F. Göktepe, Ö. Göktepe, S. M. Mirvakili, S. Naficy, X. Lepró, J. Oh, M. E. Kozlov, S. J. Kim, X. Xu, B. J. Swedlove, G. G. Wallace, and R. H. Baughman, "Artificial muscles from fishing line and sewing thread," *Science*, vol. 343, no. 6173, pp. 868–872, 2014.
- [6] S. Kianzad, J. D. Pandit, Milind Lewis, A. R. Berlingeri, K. J. Haebler, and J. D. Madden, "Variable stiffness and recruitment using nylon actuators arranged in a pennate configuration," in *Proceedings of SPIE on Electroactive Polymer Actuators and Devices (EAPAD)*, vol. 9430, 2015.
- [7] K. H. Cho, M. G. Song, H. Jung, J. Park, H. Moon, J. C. Koo, J.-D. Nam, and H. R. Choi, "A robotic finger driven by twisted and coiled polymer actuator," in *Proceedings of SPIE Electroactive Polymer Actuators and Devices (EAPAD)*, vol. 9798, 2016.
- [8] M. C. Yip and G. Niemeyer, "On the control and properties of supercoiled polymer artificial muscles," *IEEE Trans. Robot.*, vol. 33, no. 3, pp. 689–699, 2017.
- [9] B. Pawlowski, J. Sun, J. Xu, Y. Liu, and J. Zhao, "Modeling of soft robots actuated by twisted-and-coiled actuators," *IEEE/ASME Transactions on Mechatronics*, vol. 24, no. 1, pp. 5–15, 2019.
- [10] L. Sutton, H. Moein, A. Rafiee, J. D. W. Madden, and C. Menon, "Design of an assistive wrist orthosis using conductive nylon actuators," in *Proceedings of IEEE International Conference on Biomedical Robotics and Biomechatronics (BioRob)*, 2016, pp. 1074–1079.
- [11] M. Hiraoka, K. Nakamura, H. Arase, K. Asai, Y. Kaneko, S. W. John, K. Tagashira, and A. Omote, "Power-efficient low-temperature woven coiled fibre actuator for wearable applications," *Scientific Reports*, vol. 6, 2016.
- [12] Y. Almubarak and Y. Tadesse, "Twisted and coiled polymer (TCP) muscles embedded in silicone elastomer for use in soft robot," *International Journal of Intelligent Robotics and Applications*, 2017.
- [13] L. Wu, M. J. de Andrade, L. K. Saharan, R. S. Rome, R. H. Baughman, and Y. Tadesse, "Compact and low-cost humanoid hand powered by nylon artificial muscles," *Bioinspiration & Biomimetics*, vol. 12, no. 2, p. 026004, 2017.
- [14] A. Simeonov, T. Henderson, Z. Lan, G. Sundar, A. Factor, J. Zhang, and M. Yip, "Bundled super-coiled polymer artificial muscles: Design, characterization, and modeling," *IEEE Robotics and Automation Letters*, vol. 3, no. 3, pp. 1671–1678, 2018.
- [15] S. M. Mirvakili, A. Rafie Ravandi, I. W. Hunter, C. S. Haines, N. Li, J. Foroughi, S. Naficy, G. M. Spinks, R. H. Baughman, and J. D. W. Madden, "Simple and strong: twisted silver painted nylon artificial muscle actuated by joule heating," in *Proceedings of SPIE Electroactive Polymer Actuators and Devices (EAPAD)*, vol. 9056, 2014
- [16] J. Weijde, B. Smit, M. Fritschi, C. Kamp, and H. Vallery, "Self-sensing of deflection, force, and temperature for joule-heated twisted and coiled polymer muscles via electrical impedance," *IEEE/ASME Transactions on Mechatronics*, vol. 22, no. 3, pp. 1268–1275, 2017.
- [17] C. S. Haines, N. Li, G. M. Spinks, A. E. Aliev, J. Di, and R. H. Baughman, "New twist on artificial muscles," *Proc. Natl. Acad. Sci. USA*, vol. 113, pp. 11709–11716, 2016.
- [18] C. Lamuta, S. Messelot, and S. Tawfick, "Theory of the tensile actuation of fiber reinforced coiled muscles," *Smart Materials and Structures*, vol. 27, no. 5, p. 055018, 2018.
- [19] J. Zhang, K. Iyer, A. Simeonov, and M. C. Yip, "Modeling and inverse compensation of hysteresis in super-coiled polymer artificial muscles," *IEEE Robot. Autom. Lett.*, vol. 2, no. 2, pp. 773–780, 2017.
- [20] K. K. Leang, Q. Zou, and S. Devasia, "Feedforward control of piezoactuators in atomic force microscope systems," *IEEE Control Systems*, vol. 29, no. 1, pp. 70–82, 2009.

- [21] X. Tan and J. Baras, "Modeling and control of hysteresis in magnetostrictive actuators," *Automatica*, vol. 40, no. 9, pp. 1469–1480, 2004
- [22] R. Iyer and X. Tan, "Control of hysteretic systems through inverse compensation," *IEEE Control Systems Magazine*, vol. 29, no. 1, pp. 83–99, 2009.
- [23] S. Shao, M. Xu, S. Zhang, and S. Xie, "Stroke maximizing and high efficient hysteresis hybrid modeling for a rhombic piezoelectric actuator," *Mechanical Systems and Signal Processing*, vol. 75, pp. 631–647, 2016.
- [24] J. Zhang, E. Merced, N. Sepúlveda, and X. Tan, "Modeling and inverse compensation of non-monotonic hysteresis in VO₂-coated microactuators," *IEEE/ASME Transactions on Mechatronics*, vol. 19, no. 2, pp. 579–588, 2014.
- [25] J. Zhang, A. Simeonov, and M. C. Yip, "Three-dimensional hysteresis compensation enhances accuracy of robotic artificial muscles," *Smart Materials and Structures*, vol. 27, no. 3, p. 035002, 2018.
- [26] I. Mayergoyz, Mathematical models of hysteresis. Springer-Verlag, 1991.
- [27] J. D. W. Madden and S. Kianzad, "Twisted lines: Artificial muscle and advanced instruments can be formed from nylon threads and fabric." *IEEE Pulse*, vol. 6, no. 1, pp. 32–35, 2015.
- [28] H. Tanizaki, K. Takagi, C. Oiwa, K. Masuya, K. Tahara, T. Irisawa, M. Shioya, and K. Asaka, "Experimental investigation of temperature-dependent hysteresis of fishing-line artificial muscle (twisted and coiled polymer fiber) actuator," in *Proceedings of SPIE: Electroactive Polymer Actuators and Devices (EAPAD)*, vol. 10966, 2019.
- [29] T. A. Luong, S. Seo, J. C. Koo, H. R. Choi, and H. Moon, "Differential hysteresis modeling with adaptive parameter estimation of a supercoiled polymer actuator," in *Proceedings of International Conference* on Ubiquitous Robots and Ambient Intelligence (URAI), 2017, pp. 607–612.
- [30] M. C. Yip and G. Niemeyer, "High-performance robotic muscles from conductive nylon sewing thread," in *Proceedings of IEEE International Conference on Robotics and Automation (ICRA)*, 2015, pp. 2313– 2318.